JACS
JOURNAL OF THE AMERICAN CHEMICAL SOCIETY

COMMUNICATION

pubs.acs.org/JACS

Relating Rates of Catalyst Sintering to the Disappearance of Individual Nanoparticles during Ostwald Ripening

Sivakumar R. Challa,[†] Andrew T. Delariva,[†,‡] Thomas W. Hansen,[†,‡,§] Stig Helveg,[‡] Jens Sehested,[‡] Poul L. Hansen,[‡] Fernando Garzon,[∥] and Abhaya K. Datye*[,†]

[†]University of New Mexico, Albuquerque, New Mexico 87131, United States

[‡]Haldor Topsøe A/S, Nymøllevej 55, DK-2800 Kgs. Lyngby, Denmark

[§]Center for Electron Nanoscopy, Technical University of Denmark, 2800 Kgs. Lyngby, Denmark

[∥]Los Alamos National Laboratory, Los Alamos, New Mexico 87545, United States

Supporting Information

ABSTRACT: Sintering of nanoparticles (NPs) of Ni supported on $MgAl_2O_4$ was monitored in situ using transmission electron microscopy (TEM) during exposure to an equimolar mixture of H_2 and H_2O at a pressure of 3.6 mbar at 750 °C, conditions relevant to methane steam reforming. The TEM images revealed an increase in the mean particle size due to disappearance of smaller, immobile NPs and the resultant growth of the larger NPs. A new approach for predicting the long-term sintering of NPs is presented wherein microscopic observations of the ripening of individual NPs (over a span of a few seconds) are used to extract energetic parameters that allow a description of the collective behavior of the entire population of NPs (over several tens of minutes).

Catalyst sintering is one of the dominant causes of deactivation in industrial heterogeneous catalysts.[1,2] Sintering refers to the increase in mean particle size that occurs as the system of nanoparticles (NPs) attains a lower-energy state (also termed coarsening, or grain growth in the ceramics literature). The driving force for catalyst sintering is the increased surface free energy of NPs in comparison with bulk metal surfaces. Sintering is particularly acute in catalysts such as automotive exhaust catalysts[3,4] and catalysts used for steam reforming of methane that operate at elevated temperatures.[5,6] Ostwald ripening, one of the mechanisms of sintering, is also responsible for the dissolution of Pt NPs and their redistribution that occurs in fuel cell electrocatalysts.[7] While several models have been proposed to describe the kinetics of catalyst sintering,[1,8] they are often more useful for correlating observed sintering rates than for describing the basic energetics of the gas−metal−support interface. Furthermore, most observations of industrial catalysts are performed before or after use (ex situ), which makes it difficult to infer the mechanisms responsible for catalyst sintering. In this work, we present observations of catalyst sintering via in situ transmission electron microscopy (TEM) that provide direct information about the mechanism of sintering. The observed rates of disappearance of individual NPs have allowed us to extract energetic parameters that help describe the evolution of the entire assembly of NPs. This method is generally applicable to a broader range of catalyst systems and reaction environments and may thus provide a more fundamental approach for understanding and predicting the long-term behavior of catalytic materials.

Previous work on NPs has helped to establish the validity of the Ostwald ripening theory for several supported NP systems.[1,8] Sambles et al.[9] studied the evaporation of individual Ag and Pb NPs supported on carbon substrates and confirmed the applicability of the Gibbs−Thomson equation (also known as the Kelvin equation) for calculating the rate of evaporation. Yang et al.[10] studied the sintering of Au NPs on $TiO_2(110)$ and were able to explain the observed evolution of particle sizes using a ripening model. More recently, by using a model thin-film catalyst, Simonsen et al.[11] confirmed that Ostwald ripening is responsible for the sintering of Pt under oxidative atmospheres. Since Pt is known to form a volatile oxide, it is plausible that this Pt oxide constitutes the mobile phase responsible for Pt sintering. Several previous studies have shown that Ostwald ripening may play a role in catalyst sintering, but all of these studies were performed on *model catalysts*.

Industrial catalysts are considerably more heterogeneous in structure and are operated at elevated temperatures in the presence of reactive gases. There is still a debate about the operative mechanism for catalyst sintering in industrial catalysts.[12] Establishing the mechanisms of sintering in industrial catalysts is more difficult because the operating conditions (high temperatures and pressures) make in situ studies difficult. Hence, most published work relevant to industrial catalysts involves observations before and after catalyst aging.[4,6,13] As in situ capabilities are now available in TEM, it has become possible to perform sintering studies under conditions approaching those used in industrial practice,[14] albeit limited in pressure to the 1−1000 mbar range and in time to the scale of hours. Thus, linking the in situ observations of sintering over the short time scales to catalyst sintering covering hundreds of hours in technical applications remains a challenge. This is indeed the goal of the present work, in which the kinetics of disappearance of individual NPs have been used to predict the evolution of particle sizes over a longer time interval.

In this work, we used in situ TEM to study the sintering of a methane steam reforming catalyst consisting of Ni NPs supported on $MgAl_2O_4$.[15] In brief, the NPs were exposed to conditions

Received: September 2, 2011
Published: November 16, 2011

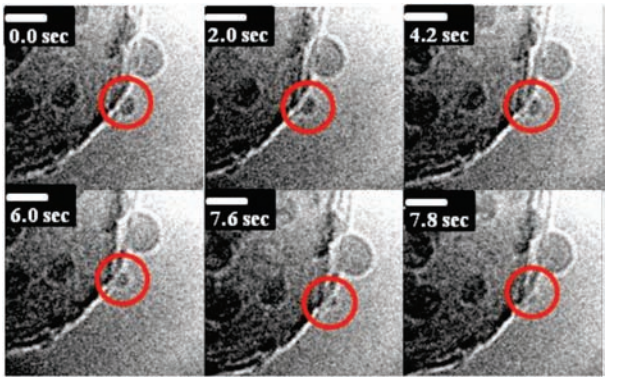

Figure 1. Time-lapsed TEM images of $MgAl_2O_4$-supported Ni NPs at 750 °C in 1:1 H_2/H_2O at a total pressure of 3.6 mbar. The scale bars in the images represent 5 nm, and the times relative to the start of observation (which was within a few minutes of reaching the operating temperature) are indicated.

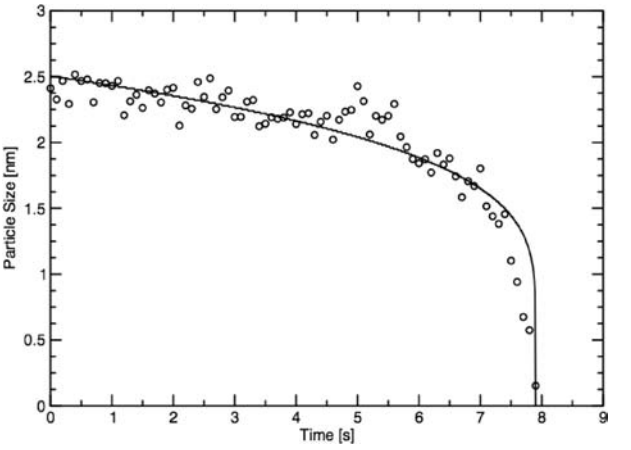

Figure 2. Size evolution of the Ni NP in Figure 1: experimental data (○) and best-fit predictions based on eq 3 (solid line).

relevant to steam reforming of methane[6,13] (e.g., a 1:1 mixture of H_2 and H_2O at a total pressure of ca. 3.6 mbar heated to 750 °C for up to 3 h), and the sintering behavior was captured as single images and time-lapsed image series. The details of sample preparation and TEM specifications can be found in the Supporting Information (SI).[15] The time-lapsed TEM image series (beam-on experiments) gave direct information about the Ni NP dynamics during exposure to the aging environment. Figure 1 shows frames from one such image series (see the SI) revealing that small particles remained immobile and decreased in size at a steady rate, followed by a dramatic increase in the rate of change of NP size in the final stages. These observations are characteristic of Ostwald ripening. The larger NPs in the vicinity of the shrinking NP did not appear to grow, as expected for ripening-mediated sintering. However, over short time intervals, such as the 8 s period in Figure 1, a relative change in mass of the smaller NPs was more readily detectable than that of the larger ones, for which the change may not have been captured reliably in the projected images. Single TEM images of specific areas of the catalysts acquired at 30 min intervals (beam-off experiments) confirmed that there was indeed an increase in the mean NP size and that the total mass appeared to be conserved. While most of the observed events seemed to be consistent with Ostwald ripening of the Ni, a few events of NP migration and coalescence were also observed to cause particle sintering. Further experimental details and movie sequences are reported elsewhere.[15]

From the images in the time-lapsed series corresponding to Figure 1, the size of the NP, viewed in profile, was determined as a function of time. The size is defined as the longest chord (see the SI for more details). The temporal evolution of the NP size (Figure 2) comprises a steady decrease in size over the first few seconds followed by a rapid decrease once the size fell below 1.5 nm. The rapid decrease caused the particle to last less than 1 s once its size fell below a critical value. Several instances of such fast decay of smaller NPs were observed in our work on Ni NPs. The variation in size from frame to frame, superimposed on the overall particle decay, is on the order of one atomic diameter and is attributed to the experimental error in the size estimation and to residual sample drift, which caused sample motion during the CCD exposure time.

Since a temporal trajectory similar to that in Figure 2 would be expected for the evaporation of Ni NPs, we first analyzed whether this decrease in particle size could be explained by evaporation of Ni. The decrease in size for evaporation of a metal particle can be computed using the approach first proposed by Langmuir.[16] Using the vapor pressure of Ni[17] and its surface tension[18] and modifying Langmuir's equation to include the Gibbs−Thomson effect, we estimated that it would take ∼130 h for a 2.5 nm particle of Ni to disappear completely (see the SI). In the presence of a gas it will take even longer for the particle to disappear.[19] Thus, in view of the fact that a 2.5 nm Ni particle in the in situ study vanished in <10 s, it is clear that the disappearance was due to surface ripening rather than evaporation. Dissolution of Ni into the support was unlikely under these experimental conditions.

There are two widely employed mean-field models of surface ripening: interface-controlled ripening and diffusion-controlled ripening. In the former model, movement of adatoms across the particle−substrate interface constitutes the rate-determining step for transport of adatoms between supported particles. In the latter model, the diffusion of adatoms on the substrate is assumed to be the rate-determining step. Since for typical coinage metals the activation barrier for emission of metal atoms onto oxide substrates is high (∼2.5 eV) and the diffusion of adatoms on substrates (barriers of 0.2−0.5 eV) is fast,[20a,b] we assume that interface-controlled surface ripening kinetics govern the overall ripening in the present system. The relation governing the NP radius r in this case is given by[1,2,21]

$$\frac{dr}{dt} = \frac{2\nu\Omega \sin\theta}{a(2 - 3\cos\theta + \cos^3\theta)} \exp\left(-\frac{E_{tot}}{k_B T}\right)\left(\frac{1}{r}\right) \times \left[\exp\left(\frac{2\gamma\Omega}{r^* k_B T}\right) - \exp\left(\frac{2\gamma\Omega}{r k_B T}\right)\right] \quad (1)$$

where θ is the contact angle of the supported particle, a is the interatomic distance, ν is the frequency of thermal vibration of atoms in a lattice, and k_B is the Boltzmann constant. The apparent activation energy for ripening, E_{tot}, is given by $E_{tot} = \Delta H_{sub} - E_{ads} + E_{diff}$, where ΔH_{sub} is the heat of sublimation of the metal, E_{ads} is the energy of adsorption of a metal adatom on the substrate, and E_{diff} is the activation energy for diffusion of the adatom on the substrate surface. The first exponential inside the brackets corresponds to the surface concentration of adatoms in the mean field, with r^* being the size of a hypothetical NP that is in equilibrium with the collection of NPs undergoing sintering and that is neither decreasing nor increasing in size. The second exponential corresponds to the concentration of adatoms in the vicinity of a particle of radius r. These exponential terms arise

from the dependence of the surface free energy on the particle size, as described by the Gibbs−Thomson (or Kelvin) relation. In a simpler form with all of the constant prefactors combined into a constant K_{int}, the relation is given by

$$\frac{dr}{dt} = \frac{K_{int}}{r}\left[\exp\left(\frac{2\gamma\Omega}{r^* k_B T}\right) - \exp\left(\frac{2\gamma\Omega}{r k_B T}\right)\right] \quad (2)$$

In principle, the above kinetic relation requires the knowledge of the sizes of all the NPs making up the system to enable the calculation of r^*. However, for the smallest NPs in the system, the rate of change of the NP size is predominantly determined by the rate of emission of adatoms from this NP onto the substrate, and we assume that the number of adatoms being received by the shrinking NP is negligible since the surrounding NPs are much larger. A similar argument was used to model the disappearance of gold NPs on TiO_2.[10] With this simplification, eq 2 reduces to

$$\frac{dr}{dt} = -\frac{K_{int}}{r}\exp\left(\frac{2\gamma\Omega}{r k_B T}\right) \quad (3)$$

which describes the decay of an individual NP. This equation was integrated numerically using the physical parameters of nickel to model the decay of a 2.5 nm NP. The value of r^* was comparatively large for the initial particle size distribution ($d^* = 2r^* = 6$ nm; see below). The best fit between the experimental decay rates and the ripening model was obtained using only one adjustable constant, $K_{int} = 4.98 \times 10^{-3}$ nm^2/s, corresponding to an activation energy for ripening (E_{tot}) of 264.5 kJ/mol. This E_{tot} was obtained from the fit to the experimental data by assuming the NPs to be hemispherical ($\theta = 90°$; see the SI) and using $a = 0.276$ nm and $\nu = 4 \times 10^{12}$ Hz (ν is usually $10^{12}-10^{14}$ Hz[21,22]). As an aside, on the basis of the value ΔH_{sub} = 430 kJ/mol for Ni[17] and typical estimates of $E_{ads} \approx$ 2.0 eV and $E_{diff} \approx 0.2-0.5$ eV for metals (Ag, Pt, Pd)[20] on alumina, E_{tot} can be estimated as 250−280 kJ/mol, which compares reasonably well with the value obtained from the fit to the data. The best-fit decay is included in Figure 2 and matches the experimental decay reasonably well at all times of the existence of this NP. Additional analyses that included the effect of r^* indicated that the assumption of $r < r^*$ used to obtain eq 3 from eq 2 was well justified and led to insignificant effects on the fit results (see Figure S2 and the accompanying discussion in the SI).

As mentioned earlier, a similar rapid change in particle size was reported in the literature during evaporation of supported metal particles,[9] and during the decay of monatomic high (2D) metal islands on terraces.[23] To our knowledge, this is the first report of the direct observation of the decay of individual NPs in an industrially relevant catalyst whose rate of disappearance has been explained based on the Ostwald ripening model. A linearized version of the Gibbs−Thomson equation obtained by approximating e^x as $1 + x$, as assumed in the classical Ostwald ripening models,[1,8] led to a poor fit to the data (Figure S3). At 750 °C, the values of the physical parameters γ and Ω for Ni gave an exponent $x > 2.2$, which clearly indicates the inapplicability of the linearization.

Equation 3 can be written in the following form, which is useful for data fitting:

$$\frac{dr}{dt} = -\frac{K}{r}\exp\left(\frac{r_c}{r}\right)$$

where K and r_c are constants that can be obtained from the decay of individual particles. The parameter r_c is akin to the capillary length and can give additional insights into the species involved in the ripening, such as its interfacial energy (e.g., see studies of 2D nanostructure ripening[23]). The prefactor K is related to the apparent activation barrier for sintering,[2,10] which includes the effect of the gaseous environment in which the sintering occurs.[13,24]

The robustness of the fit was tested by varying E_{tot} by ±5−10 kJ/mol, corresponding to factors of 1.8−3.2 for K_{int}. As illustrated in Figure S4, the model is sensitive to the value of K_{int}. Lowering E_{tot} by 5 kJ/mol almost halved the lifetime of a 2.5 nm particle to 4 s. On the other hand, an increase in the barrier by 5−10 kJ/mol prolonged the ripening by a factor of 2−3. When the predicted NP sizes were rescaled to portray a common moment of disappearance (set to the in situ time), the employed variation in the activation barrier for ripening indicated the possibility of a 0.3−0.6 nm variation in the initial size (Figure S5), which is comparable to the resolution of the microscope used in the in situ study[15] (see the SI). Therefore, the values of E_{tot} (or K_{int}) derived from the fit shown in Figure 2 can be considered reliable for describing the NP decay kinetics. In addition, several other Ni NPs on similar experimental samples were successfully fitted using E_{tot}=264.5 ± 15 kJ/mol, corresponding to $K_{int} = 4.98 \times 10^{-3}$ nm^2/s (see Figures S6 and S7 and the accompanying discussion in the SI). This is indicative of both the predominance of the mechanism of ripening and the reproducibility of the ripening behavior.

Next, the ripening model was employed to predict the extent of sintering in a collection of NPs. As an experimental reference, single TEM images of specific areas of the specimen were acquired initially after the aging conditions were established and subsequently after 30 min of aging in the in situ experiment with the electron illumination switched off (beam-off experiment). The particle diameters were obtained from the TEM images. With the observed initial NP size distribution as the initial size distribution, eq 2 was integrated numerically for an initial ensemble of 5000 NPs using a small time step (0.001 s) with the fitted K_{int} value of 4.98×10^{-3} nm^2/s, and the calculation of the critical size r^* (see eq 2) at every time-step was based on a mass-conserving definition.[25] Figure 3 shows the predicted size distribution of Ni particles after 30 min. Roughly 40% of the NPs (1897) remain after 30 min. The predicted size distribution is very close to the observed distribution. Scatter in the predicted size distribution is seen because the initial distribution was obtained from experimental images and hence contains the scatter typical for experimental data (depicted by the black dots in Figure 3). The predicted size distribution after 30 min of sintering is remarkable because it has a pronounced tail to the right and fits well to a log-normal distribution. The log-normal distribution function fits indicate average NP sizes of 8.4 and 7.7 nm (5.75 nm initially) for the predicted and observed size distributions, respectively, after 30 min of sintering. The ripening model combined with the derived physical parameters is therefore able to describe reasonably well the behavior in the initial periods of catalyst sintering under the present conditions.

It is worth pointing out that the analyses presented herein are based on a model (eq 1) relying on assumptions of mean-field and continuum behavior.[1,8] Studies have shown that local concentration effects[11,23b] and particle-size energetics (varying metal surface tension and heats of sublimation) influenced by atomic-scale surface heterogeneities[2,26] can affect metal NP sintering, in addition to other effects such as support instabilities and hot spots in a catalyst bed. These factors will definitely affect the predictions of long-term catalyst sintering. However, the inherent assumptions of the employed model should not impact the approach of parametrization

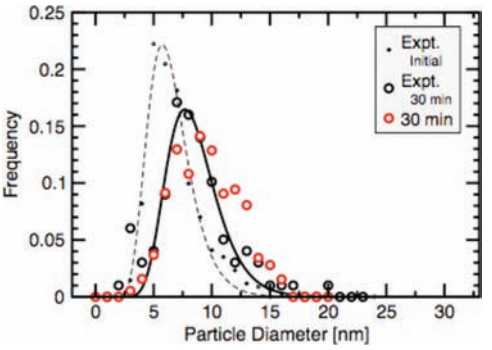

Figure 3. Size distributions before and after ripening for 30 min: experimental (black dots, initial; circles, after 30 min) and as predicted by eq 2 (red circles). The smooth curves are fits to the experimental data (broken-line, initial; solid-line, after 30 min) using a log-normal distribution.

of the experimental data to obtain the energetics of the gas–metal–support interface.

In summary, sintering of Ni NPs supported on $MgAl_2O_4$ was studied via in situ TEM under conditions relevant to steam reforming of methane. The TEM images showed that smaller Ni NPs shrank in size and disappeared within a few seconds at 750 °C. As this decay was much faster than predicted by the rates of evaporation of the metal, the observations of NP decay are indicative of ripening. The accelerated decay of particles with time is consistent with the increase in surface chemical potential predicted by the Gibbs–Thomson equation. The decay in size of a limited number of NPs was analyzed using the formalism of Ostwald ripening to derive the activation energy for ripening. The activation energy was then used to predict the evolution of the particle size distribution during longer term (30 min) aging of the catalyst, which matched well the observed change for an ensemble of NPs. This finding suggests that ripening dominates the sintering in the ensemble of NPs.

Accelerated aging performed at higher temperatures for shorter time periods to help predict the long-term behavior of catalysts often leaves the fundamental parameters undetermined. Our work shows that short-term in situ TEM observations may provide a method suitable for generating some of those fundamental parameters. The influence of the electron beam dose rates on the dynamics of particle disappearance were not investigated in as much detail as in ref 11. However, we expect limited impact due to beam damage since there was good agreement between the model predictions made with parameters derived with the beam-on experiments and the results of longer-term beam-off experiments. The applicability of this approach for modeling of the long-term sintering behavior at higher operating pressures still remains to be addressed, and this may call for some adjustments because the sintering kinetics are expected to be dependent on the pressure and composition of the gas phase.[13] In view of the ubiquity of NPs in numerous areas of technology, this work can provide a method for understanding the growth kinetics and stability in other systems as well as predicting the long-term behavior of industrial catalysts.

■ ASSOCIATED CONTENT

Ⓢ Supporting Information. Movie (AVI) associated with Figure 1, Figures S1–S7, and complete references. This material is available free of charge via the Internet at http://pubs.acs.org.

■ AUTHOR INFORMATION

Corresponding Author
datye@unm.edu

■ ACKNOWLEDGMENT

Financial support from the DOE–EERE Office of Fuel Cell Technology is gratefully acknowledged. We also acknowledge support from Haldor Topsøe A/S and the participation of the CTCI Foundation, Taiwan, in the establishment of the in situ TEM facility used in this study. A.T.D. and A.K.D. acknowledge financial support from NSF Grants CTS-0500471 and OISE-0730277.

■ REFERENCES

(1) Wynblatt, P.; Gjostein, N. A. *Prog. Solid State Chem.* **1975**, *9*, 21.
(2) Campbell, C. T.; Parker, S. C.; Starr, D. E. *Science* **2002**, *298*, 811.
(3) Datye, A. K.; et al. *Catal. Today* **2006**, *111*, 59.
(4) Xu, Q.; et al. *ChemCatChem* **2011**, *3*, 1004.
(5) Rostrup-Nielsen, J. R. In *Catalysis: Science and Technology*; Anderson, J. R., Boudart, M., Eds.; Springer: Berlin, 1984; Vol. 5, Chapter 1.
(6) Sehested, J.; et al. *J. Catal.* **2001**, *197*, 200.
(7) (a) Borup, R.; et al. *Chem. Rev.* **2007**, *107*, 3904. (b) Mayrhofer, K. J. J.; et al. *J. Power Sources* **2008**, *185*, 734.
(8) Chakraverty, B. K. *J. Phys. Chem. Solids* **1967**, *28*, 2401.
(9) Sambles, J. R.; et al. *Proc. R. Soc. London, Ser. A.* **1970**, *318*, 507.
(10) Yang, F.; et al. *J. Phys. Chem. C* **2009**, *113*, 254.
(11) Simonsen, S. B.; et al. *J. Am. Chem. Soc.* **2010**, *132*, 7968.
(12) (a) Granqvist, C. G.; Buhrman, R. A. *J. Catal.* **1976**, *42*, 477. (b) Wanke, S. E. *J. Catal.* **1977**, *46*, 234. (c) Granqvist, C. G.; Buhrman, R. A. *J. Catal.* **1977**, *46*, 238. (d) Richardson, J. T.; Crump, J. G. *J. Catal.* **1979**, *57*, 417.
(13) Sehested, J.; et al. *J. Catal.* **2004**, *223*, 432.
(14) (a) Baker, R. T. K.; et al. *Surf. Sci.* **1974**, *46*, 311. (b) Liu, R.-J.; et al. *Appl. Catal., A* **2005**, *282*, 111.
(15) Delariva, A. Ph.D. Dissertation, University of New Mexico, Albuquerque, NM, 2010.
(16) Langmuir, I. *Phys. Rev.* **1913**, *2*, 329.
(17) *CRC Handbook of Chemistry and Physics*, Internet ed.; Lide, D. R., Ed.; CRC Press: Boca Raton, FL, 2005.
(18) *CRC Handbook of Materials Science, Volume I: General Properties*; Lynch, C. T., Ed.; CRC Press: Boca Raton, FL, 1986.
(19) Fonda, G. R. *Phys. Rev.* **1923**, *21*, 343.
(20) (a) Meyer, R.; et al. *Surf. Sci.* **2007**, *601*, 134. (b) Deskins, N. A.; et al. *Surf. Sci.* **2009**, *603*, 2793. (c) Valero, M. C.; et al. *Phys. Rev. B* **2007**, *75*, No. 045427.
(21) Parker, S. C.; Campbell, C. T. *Phys. Rev. B* **2007**, *75*, No. 035430.
(22) Venables, J. A. *Introduction to Surface and Thin Film Processes*; Cambridge University Press: Cambridge, U.K., 2000.
(23) (a) Morgenstern, K.; et al. *Phys. Rev. Lett.* **1996**, *76*, 2113. (b) Bartelt, N. C.; et al. *Phys. Rev. B* **1996**, *54*, 11741.
(24) Wynblatt, P.; Gjostein, N. A. *Acta Metall.* **1976**, *24*, 1165.
(25) Houk, L. R.; et al. *Langmuir* **2009**, *25*, 11225.
(26) (a) Luo, W.; et al. *J. Phys. Chem. C* **2008**, *112*, 2359. (b) Safaei, A. *J. Phys. Chem. C* **2010**, *114*, 13482.